Supplement of Atmos. Chem. Phys., 25, 9031–9060, 2025
https://doi.org/10.5194/acp-25-9031-2025-supplement

Atmospheric Chemistry and Physics
Open Access
EGU

Supplement of

Climate forcing due to future ozone changes: an intercomparison of metrics and methods

William J. Collins et al.

Correspondence to: William J. Collins (w.collins@reading.ac.uk) and Fiona M. O'Connor (f.m.oconnor@exter.ac.uk)

Supplementary materials

S1 Participating Models (CESM2, EMAC, GFDL-ESM4, GISS-E2.1, NorESM2, UKESM1-0-LL, GEOS-Chem)

The Community Earth System Model version 2 (CESM2) used here is described in detail by Danabasoglu et al. (2020). We use the Community Atmosphere Model version 6 with Chemistry (CAM6-Chem) configuration of CESM2 with a nominal 1° horizontal resolution, 32 hybrid sigma-pressure vertical levels and a model top at 2.26 hPa. CAM6 calculates radiative transfer by the correlated k-distribution method via the Rapid Radiative Transfer Model for General circulation models code (RRTMG) (Iacono et al., 2008)). Tropospheric and stratospheric chemistry is based on the Model for Ozone and Related chemical Tracers (MOZART) family of chemical mechanisms with a comprehensive chemical mechanism in the troposphere and stratosphere (MOZART-TS1) (Emmons et al., 2020), including a comprehensive Volatility Basis Set (VBS) parameterisation for the formation of Secondary Organic Aerosols (Tilmes et al., 2019) and the MAM4 modal aerosol model (Liu et al., 2016). The chemical mechanism includes 221 species with 405 gas-phase reactions and 123 photolysis reactions.

The ECHAM/ Modular Earth Submodel System (MESSy) Atmospheric Chemistry (EMAC) model is comprised of the core atmospheric model ECHAM5 (5th generation European Centre Hamburg general circulation model) (Roeckner et al., 2006), and the Modular Earth Submodel system, MESSy, as described by Jöckel et al. (2010). The overall model setup applied in the present study is very similar to the EMAC simulations performed for CCMI-2, which are an update of the setups described by (Jöckel et al., 2016). EMAC (MESSy version d2.55.2-5109) is applied in the T42L90MA-resolution, i.e. with a spherical truncation of T42 (corresponding to a quadratic Gaussian grid of approx. 2.8° by 2.8° in latitude and longitude) with 90 vertical hybrid pressure levels up to 0.01 hPa. For the chemical kinetics, the submodel MECCA (Module Efficiently Calculating the Chemistry of the Atmosphere) (Sander et al., 2019) is used. The chemical mechanism considers the basic gas-phase chemistry of ozone, methane, and odd nitrogen. Alkanes and alkenes are included up to C4. Alkynes and aromatics are not considered in our mechanism. Halogen chemistry includes bromine and chlorine species. For the chemistry of isoprene plus a few selected non-methane hydrocarbons (NMHCs), we used version 1 of the Mainz Isoprene Mechanism (MIM1) based on Pöschl et al. (2000). Aqueous-phase kinetics, ice-phase kinetics and wet deposition have been calculated with the submodel SCAV (Tost et al., 2006). Heterogeneous reaction rates on stratospheric aerosol and polar stratospheric clouds were simulated using the submodel MSBM (Jöckel et al., 2016; Kirner et al., 2011). In total, 265 gas phase, 159 aqueous phase, 3 ice phase, 82 photolysis and 12 heterogeneous reactions for 204 chemical species are considered. Radiation is calculated based on the ECHAM5 radiation scheme, i.e. RRTM in the LW and the Fouquart and Bonnel (1980) scheme in the SW plus FUBrad (Kunze et al.,

2014), as described by Dietmüller et al. (2016) with the MESSy submodel RAD, which allows for multiple diagnostic radiation calls (Dietmüller et al., 2016; Nützel et al., 2024).

The GFDL Earth System Model version 4 (GFDL-ESM4) is documented by Dunne et al. (2020), using the atmospheric component AM4.1 as described by Horowitz et al. (2020). The base configuration used here is the same as that used for Phase 6 of the Coupled Model Intercomparison Project (Eyring et al., 2016). Briefly, the model has a horizontal resolution of approximately 100 km (~ 1° latitude by 1° longitude), using the GFDL Finite-Volume Cubed-Sphere dynamical core (Harris and Lin, 2013; Putman and Lin, 2007), with 49 hybrid sigma-pressure vertical levels extending from the surface to 1 Pa (~80 km). AM4.1 includes interactive tropospheric and stratospheric gas-phase and aerosol chemistry. The combined tropospheric and stratospheric chemistry scheme includes 18 prognostic (transported) bulk aerosol tracers, 58 prognostic gas-phase tracers, five prognostic idealised tracers, and 40 diagnostic (non-transported) chemical tracers, with 43 photolysis reactions, 190 gas-phase kinetic reactions, and 15 heterogeneous reactions. The tropospheric chemistry includes reactions of the NO_x–HO_x–O_x–CO–CH_4 system and oxidation schemes for other non-methane volatile organic compounds. The stratospheric chemistry accounts for the major ozone loss cycles (O_x, HO_x, NO_x, ClO_x, and BrO_x) and heterogeneous reactions on ice and nitric acid trihydrate polar stratospheric clouds (PSCs) and in liquid ternary solution (LTS) aerosols. Emissions of biogenic volatile organic compounds (VOCs), dust, sea salt, dimethyl sulphide (DMS), marine organic aerosols, and lightning NO_x are calculated interactively as a function of model meteorology. The radiation scheme in GFDL-ESM4 has been comprehensively updated in the SW (Exponential Sum Fit scheme; ESF) and LW (Simplified Exchange Approximation scheme; SEA); a full description can be found in Zhao et al. (2018). The land component (LM4.1) of the model uses an interactive dynamic vegetation scheme to simulate vegetation dynamics (Shevliakova et al., 2024).

This study used version 2.1 of the GISS ModelE Earth system model, ModelE2.1 (GISS-E2.1), as described and evaluated for the present day (Kelley et al., 2020), historical period (Miller et al., 2021) and in future projections (Nazarenko et al., 2022). The horizontal and vertical resolution of the atmosphere in ModelE2.1 is 2° in latitude by 2.5° in longitude with 40 vertical layers from the surface to 0.1 hPa. The radiative transfer model is described by (Lacis and Oinas, 1991). Tropospheric chemistry (Shindell et al., 2001, 2003) includes the inorganic chemistry of reactive oxygen (O_x), nitrogen (NO_x), and hydrogen (HO_x) families as well as carbon monoxide (CO), and the organic chemistry of methane and higher hydrocarbons using a modified Carbon Bond Mechanism version 4 (CBM4) scheme (Gery et al., 1989). The stratospheric chemistry includes chlorine and bromine chemistry together with polar stratospheric clouds (Shindell et al., 2006). The original chemical scheme has been updated and evaluated since its first implementation (Shindell et al., 2013) and has continued to be updated since (Rivera et al., 2024). ModelE2.1 includes multiple aerosol schemes (Bauer et al., 2020): One-Moment Aerosols (OMA), which is the scheme used here, is fully interactive within ModelE2.1 in terms of emissions, chemistry, transport, removal, and climate.

Aerosol-radiation interactions (ARIs) and aerosol-cloud interactions (ACIs) are calculated within the radiation and cloud schemes, where the size-dependent scattering properties of clouds and aerosols are computed from Mie scattering. Apart from swelling with water, there is no internal mixing in OMA radiative calculations - all aerosols are regarded as externally mixed.

The Norwegian Earth System Model used in this study is based on the standard version of NorESM2 (Seland et al., 2020) but has been extended with comprehensive atmospheric chemistry. In this new version of NorESM2 the atmospheric aerosol scheme OsloAero (Kirkevåg et al., 2018) has been coupled with the gas-phase description of the TS1 troposphere-stratosphere chemistry scheme (Emmons et al., 2020) of CESM2. This new version now describes a total of 205 species (aerosol and gas-phase) and is currently under evaluation. As in the standard version, natural emissions of dust, isoprene and monoterpenes from land and of primary organic matter, sea-salt and DMS from the ocean are calculated interactively. The atmosphere and land components of NorESM2 used here have the same horizontal resolution of 1.9° × 2.5°, and the atmosphere contains 32 levels (up to 2.26 hPa). NorESM2 is based on CESM2 (it also uses the RRTMG radiative transfer scheme) but differs in quite some aspects. NorESM2 contains a different ocean model, a different atmospheric aerosol module (including its interactions with cloud and radiation), and modifications in the formulation of local dry and moist energy conservation, in local and global angular momentum conservation, and in the computations for deep convection and air–sea fluxes. The surface components of NorESM2 also have minor changes in their albedo calculations.

The UK's Earth System Model used in this study is based on UKESM1-0-LL (Sellar et al., 2019), as used in CMIP6. It has a horizontal resolution of 1.25° × 1.875°, with 85 hybrid height levels from the surface up to the model lid at 85 km. By default, UKESM1-0-LL includes an interactive stratosphere-troposphere chemistry scheme called StratTropv1.0 (Archibald et al., 2020) from the United Kingdom Chemistry and Aerosol (UKCA) (Morgenstern et al., 2009; O'Connor et al., 2014) model. However, near-global total column ozone was biased high relative to other CMIP6 models throughout the historical period (Keeble et al., 2021) and the stratospheric ozone response to increasing concentrations of ozone-depleting substances was too strongly negative (Morgenstern et al., 2020), resulting in UKESM1-0-LL having a negative present-day ozone forcing (Skeie et al., 2020). Here, the model simulations use UKESM1-0-LL but include an update to the chemistry scheme, i.e., StratTropv2.0 (Keeble et al.,; In preparation). In comparison with StratTropv1.0, StratTropv2.0 includes an extension to the stratospheric heterogeneous chemistry to incorporate bromine species as well as updates to bimolecular reaction rate coefficients, the treatment of the top boundary, and photolysis inputs. The radiation scheme used in UKESM1-0-LL is SOCRATES (Suite Of Community RAdiative Transfer codes based on Edwards and Slingo) which treats incoming solar radiation and thermal radiation in six SW bands and nine LW bands, respectively. A full description of SOCRATES and the physical climate model on which UKESM1-0-LL was built can be found in Walters et al. (2019). Apart from the treatment of trace gas chemistry, the configuration of UKESM1-0-LL used here is identical to that used in CMIP6.

In contrast to the other models in this study, GEOS-Chem (http://www.geos-chem.org) is a 3-D global chemistry-transport model (CTM). The model is driven by meteorological fields archived at high temporal resolution from either reanalyses or

free-running GCMs. The computational power that is not used to resolve the equations of motion is therefore applied instead to include additional chemical species and more complex chemical mechanisms. Here, version 14.4.2 of GEOS-Chem is used, whose chemistry mechanism includes 263 gas-phase and 30 condensed-phase species, undergoing 624 gas-phase, 113 heterogeneous, and 157 photolysis reactions in a unified mechanism from the surface to the mesopause, with a linearized mechanism applied in the mesosphere (e.g., Bates et al. (2024) , and ref. therein). Unlike the other simulations used in this study, the mechanism includes a comprehensive tropospheric halogen chemistry mechanism for the Br_y, Cl_y, and I_y families, which strongly influences the tropospheric ozone budget (Wang et al., 2021). The tropospheric ozone simulation was recently evaluated against observations by Wang et al. (2022). The source of NOx from lightning is described by Murray et al. (2012) and the source from soil microbes is described by Hudman et al. (2012). Biogenic VOC emissions are from version 2.1 of the Model of Emissions of Gases and Aerosols from Nature (MEGAN) inventory of Guenther et al. (2012) as implemented by Hu et al. (2015). The RRTMG radiative transfer scheme is embedded within GEOS-Chem, enabling calculation of online IRF at the surface, tropopause, and TOA from greenhouse gases and aerosol particles (Heald et al., 2014).

Report	Nominal years	Tropospheric ozone forcing	References
SAR	1850 to 1990	0.4 ± 0.2 Wm^{-2}	(Hauglustaine et al., 1994)
TAR	1850 to 1990	0.35 ± 0.15 Wm^{-2}	(Berntsen et al., 1997, 2000; Brasseur et al., 1998; Van Dorland et al., 1997; Haywood et al., 1998; Kiehl et al., 1999; Lelieveld and Dentener, 2000; Roelofs et al., 1997; Stevenson et al., 1998)
AR4	1850 to 2000	0.35 [0.25, 0.65] Wm^{-2}	(Gauss et al., 2006; Hauglustaine and Brasseur, 2001; Liao and Seinfeld, 2005; Mickley et al., 2001, 2004; Shindell et al., 2003, 2005; Wong et al., 2004)
AR5	1750 to 2010	0.4 ± 0.2 Wm^{-2}	(Skeie et al., 2011; Søvde et al., 2011; Stevenson et al., 2013)
AR6	1750 to 2019	0.45 ± 0.225 Wm^{-2}	(Skeie et al., 2020)

Table S1: Tropospheric ozone radiative forcing (calculated as SARF) from the second (SAR) to sixth IPCC Assessment Reports.

	All-sky IRF					Clear-sky IRF	
Model	Global	NH	SH	SW	LW	SW	LW
EMAC	0.267 ± 0.006	0.236 ± 0.007	0.298 ± 0.010	0.143 ± 0.004	0.123 ± 0.003	0.097 ± 0.002	0.152 ± 0.002
GEOS-Chem	0.343 ± 0.013	0.250 ± 0.011	0.436 ± 0.015	0.160 ± 0.005	0.183 ± 0.007	0.100 ± 0.000	0.232 ± 0.009
GFDL-ESM4	0.329 ± 0.004	0.258 ± 0.010	0.400 ± 0.010	0.182 ± 0.003	0.147 ± 0.003	0.125 ± 0.003	0.183 ± 0.002
GISS-E2.1_FR	0.104 ± 0.005	0.109 ± 0.014	0.100 ± 0.013	0.050 ± 0.005	0.059 ± 0.003	N/A	N/A
GISS-E2.1_nudged	-0.014 ± 0.001	0.095 ± 0.001	-0.122 ± 0.002	0.010 ± 0.001	-0.024 ± 0.001	N/A	N/A
UKESM1-0-LL	0.398 ± 0.012	0.394 ± 0.018	0.403 ± 0.015	0.217 ± 0.011	0.181 ± 0.005	0.157 ± 0.005	0.219 ± 0.005
Multi-model mean	0.288 ± 0.101	0.249 ± 0.090	0.327 ± 0.123	0.150 ± 0.056	0.139 ± 0.046	0.120 ± 0.034	0.197 ± 0.031

Table S2: Global multi-annual mean instantaneous radiative forcings (IRFs) and their standard errors for year-2050 whole atmosphere ozone relative to a year-2015 baseline (*pdClim-control*), including its SW and LW components for all-sky and clear-sky conditions based on online double radiation calls. Table also includes estimates for the northern and southern hemispheres. The multi-model means do not include GISS-E2.1_nudged and the uncertainties are the standard deviation of the model means.

Model	Global SARF	NH SARF	SH SARF	SARF SW	SARF LW	CS SARF SW	CS SARF LW
EMAC	0.191 ± 0.003	0.197 ± 0.007	0.184 ± 0.005	0.143 ± 0.004	0.047 ± 0.003	0.097 ± 0.002	0.080 ± 0.003

Table S3: Global multi-annual mean stratospherically-adjusted radiative forcing (SARF) and its standard error for year-2050 whole atmosphere ozone relative to a year-2015 baseline (*pdClim-control*) from the EMAC model, including its SW and LW components for all-sky and clear-sky conditions based on an online double radiation call for ozone and including a stratospheric temperature adjustment. Table also includes estimates for the northern and southern hemispheres.

	All-sky ERF					Clear-sky ERF	
Model	**Global**	**NH**	**SH**	**SW**	**LW**	**SW**	**LW**
CESM2	0.233 ± 0.065	0.237 ± 0.079	0.229 ± 0.068	0.201 ± 0.048	0.030 ± 0.039	0.107 ± 0.024	0.202 ± 0.027
EMAC	0.224 ± 0.005	0.180 ± 0.019	0.269 ± 0.015	0.160 ± 0.010	0.064 ± 0.006	0.110 ± 0.001	0.155 ± 0.006
GFDL-ESM4	0.298 ± 0.038	0.271 ± 0.041	0.325 ± 0.051	0.241 ± 0.031	0.058 ± 0.030	0.138 ± 0.010	0.196 ± 0.021
GISS-E2.1_FR	0.142 ± 0.047	0.163 ± 0.056	0.120 ± 0.073	0.072 ± 0.050	0.070 ± 0.061	0.016 ± 0.024	0.131 ± 0.040
GISS-E2.1_nudged	0.005 ± 0.030	0.101 ± 0.005	-0.091 ± 0.014	0.005 ± 0.005	-0.000 ± 0.003	0.005 ± 0.001	-0.031 ± 0.001
NorESM	0.297 ± 0.065	0.246 ± 0.090	0.348 ± 0.084	0.219 ± 0.057	0.078 ± 0.040	0.091 ± 0.027	0.199 ± 0.025
UKESM1-0-LL	0.415 ± 0.029	0.334 ± 0.045	0.507 ±0.046	0.491 ± 0.032	-0.076 ± 0.027	0.209 ± 0.028	0.148 ± 0.028
Multi-model mean	0.268 ± 0.084	0.238 ± 0.057	0.300± 0.118	0.231 ± 0.128	0.037 ± 0.053	0.112 ± 0.057	0.172 ± 0.028

Table S4: Global multi-annual mean effective radiative forcings and their standard errors for year-2050 whole atmosphere ozone relative to the year-2015 baseline, including its shortwave (SW) and longwave (LW) components for all-sky and clear-sky conditions. Table also includes estimates for the northern and southern hemispheres. The multi-model means do not include GISS-E2.1_nudged and the uncertainties are the standard deviation of the model means.

	SW clear	SW	LW inst. clear	LW inst.	LW adj.	NET adj.
CESM2	0.099 ± 0.003	0.141 ± 0.004	0.234 ± 0.003	0.168 ± 0.002	0.123 ± 0.002	0.265 ± 0.004
EMAC	0.112 ± 0.002	0.164 ± 0.003	0.249 ± 0.003	0.177 ± 0.002	0.076 ± 0.004	0.240 ± 0.003
GEOS-chem	0.120 ± 0.002	0.180 ± 0.003	0.326 ± 0.005	0.236 ± 0.004	0.138 ± 0.002	0.319 ± 0.005
GFDL-ESM4	0.109 ± 0.002	0.157 ± 0.002	0.226 ± 0.002	0.162 ± 0.002	0.079 ± 0.002	0.235 ± 0.002
GISS-E2.1_FR	0.035 ± 0.003	0.050 ± 0.004	0.111 ± 0.003	0.079 ± 0.002	0.084 ± 0.003	0.134 ± 0.004
GISS-E2.1_nudged	0.027 ± 0.000	0.031 ± 0.000	0.019 ± 0.000	0.002 ± 0.000	0.001 ± 0.000	0.032 ± 0.001
NorESM2	0.078 ± 0.003	0.113 ± 0.004	0.203 ± 0.005	0.145 ± 0.004	0.127 ± 0.004	0.240 ± 0.006
UKESM1-0-LL	0.175 ± 0.005	0.252 ± 0.007	0.307 ± 0.007	0.217 ± 0.006	0.025 ± 0.005	0.277 ± 0.007
Multi-model mean	0.104 ± 0.043	0.151 ± 0.062	0.236 ± 0.071	0.169 ± 0.051	0.093 ± 0.040	0.244 ± 0.057

Table S5: The radiative forcing for total ozone calculated offline using the radiative kernel as shown in Fig. 6. The results are separated for short wave clear sky (SW clear), short wave all sky (SW), long wave instantaneous clear sky (LW inst. clear), long wave instantaneous all sky (LW inst.), long wave including stratospheric temperature adjustments (LW. adj) and the net SARF (NET adj.). The uncertainty is the standard error calculated from the interannual variability. The multi-model means do not include GISS-E2.1_nudged and the uncertainties are the standard deviation of the model means. All values are in W m^{-2}.

	SW clear	SW	LW inst. clear	LW inst.	LW adj.	NET adj.
CESM2	0.025 ± 0.000	0.037 ± 0.000	0.117 ± 0.001	0.083 ± 0.001	0.128 ± 0.001	0.165 ± 0.002
EMAC	0.023 ± 0.000	0.033 ± 0.000	0.115 ± 0.001	0.081 ± 0.001	0.120 ± 0.001	0.153 ± 0.001
GEOS-chem	0.030 ± 0.000	0.044 ± 0.000	0.140 ± 0.001	0.098 ± 0.001	0.143 ± 0.001	0.186 ± 0.002
GFDL-ESM4	0.024 ± 0.000	0.035 ± 0.000	0.103 ± 0.001	0.072 ± 0.001	0.110 ± 0.001	0.144 ± 0.002
GISS-E2.1_FR	0.019 ± 0.000	0.028 ± 0.001	0.091 ± 0.002	0.064 ± 0.001	0.098 ± 0.002	0.125 ± 0.002
GISS-E2.1_nudged	0.016 ± 0.000	0.023 ± 0.000	0.082 ± 0.000	0.057 ± 0.000	0.081 ± 0.000	0.104 ± 0.000
NorESM2	0.023 ± 0.000	0.034 ± 0.001	0.109 ± 0.002	0.076 ± 0.002	0.117 ± 0.003	0.150 ± 0.003
UKESM1-0-LL	0.029 ± 0.001	0.042 ± 0.001	0.114 ± 0.003	0.079 ± 0.002	0.116 ± 0.003	0.158 ± 0.004
Multi-model mean	0.025 ± 0.004	0.036 ± 0.005	0.113 ± 0.015	0.079 ± 0.010	0.119 ± 0.014	0.155 ± 0.019

Table S6: The radiative forcing for tropospheric ozone calculated offline using the radiative kernel as shown in Fig. 6. The results are separated for short wave clear sky (SW clear), short wave all sky (SW), long wave instantaneous clear sky (LW inst. clear), long wave instantaneous all sky (LW inst.), long wave including stratospheric temperature adjustments (LW. adj) and the net SARF (NET adj.). The uncertainty is the standard error calculated from the interannual variability. The multi-model means do not include GISS_nudged and the uncertainties are the standard deviation of the model means. All values are in W m^{-2}. The tropopause is defined by the 150 nmol mol^{-1} ozone mole fraction isoline in the *pdClim-control* simulations.

	All sky Forcing					Global clear sky	
Model	**Global**	**NH**	**SH**	**SW**	**LW**	**SW**	**LW**
EMAC IRF	0.082 ± 0.003	0.099 ± 0.008	0.065 ± 0.008	0.020 ± 0.001	0.062 ± 0.001	0.018 ± 0.001	0.067 ± 0.001
GFDL-ESM4 IRF	0.168 ± 0.004	0.170 ± 0.005	0.166 ± 0.008	0.061 ± 0.003	0.107 ± 0.002	0.038 ± 0.003	0.129 ± 0.002
UKESM1-0-LL IRF	0.127 ± 0.010	0.141 ± 0.016	0.113 ± 0.012	0.049 ± 0.009	0.078 ± 0.004	0.037 ± 0.004	0.092 ± 0.004
Multi-model mean IRF	0.126 ± 0.035	0.137 ± 0.039	0.115 ± 0.041	0.043 ± 0.017	0.082 ± 0.019	0.031 ± 0.092	0.096 ± 0.025
EMAC SARF	0.144 ± 0.002	0.173 ± 0.008	0.115 ± 0.004	0.020 ± 0.001	0.124 ± 0.003	0.018 ± 0.001	0.129 ± 0.003
CESM2 ERF	0.097 ± 0.064	0.162 ± 0.081	0.032 ± 0.071	0.042 ± 0.055	0.055 ± 0.039	0.051 ± 0.021	0.183 ± 0.024
EMAC ERF	0.171 ± 0.007	0.193 ± 0.014	0.150 ± 0.022	0.062 ± 0.010	0.109 ± 0.004	0.030 ± 0.001	0.146 ± 0.005
GFDL-ESM4 ERF	0.106 ± 0.034	0.089 ± 0.047	0.124 ± 0.048	0.045 ± 0.028	0.061 ± 0.022	0.063 ± 0.011	0.142 ± 0.019
UKESM1-0-LL ERF	0.171 ± 0.028	0.209 ± 0.042	0.135 ± 0.043	0.143 ± 0.030	0.027 ± 0.029	0.057 ± 0.017	0.115 ± 0.023
Multi-model mean ERF	0.136 ± 0.035	0.163 ± 0.046	0.110 ± 0.046	0.071 ± 0.038	0.063 ± 0.029	0.050 ± 0.012	0.146 ± 0.024

Table S7: Global multi-annual mean forcings (IRF, SARF, and ERF) and their standard errors for year-2050 whole atmosphere ozone from the sensitivity simulation *pdClim-2050ssp370fODS-radO3* relative to the year-2015 baseline (*pdClim-control*), including its shortwave (SW) and longwave (LW) components for all-sky and clear-sky conditions. Table also includes estimates for the northern and southern hemispheres. Multi-model mean uncertainties are the standard deviation of the model means.

	SW clear	SW	LW inst. clear	LW inst.	LW adj.	NET adj.
CESM2	0.030 ± 0.002	0.044 ± 0.002	0.154 ± 0.002	0.112 ± 0.002	0.161 ± 0.002	0.206 ± 0.002
EMAC	0.024 ± 0.002	0.036 ± 0.002	0.134 ± 0.002	0.096 ± 0.001	0.145 ± 0.002	0.180 ± 0.002
GFDL-ESM4	0.038 ± 0.002	0.054 ± 0.002	0.134 ± 0.002	0.097 ± 0.002	0.115 ± 0.002	0.170 ± 0.002
UKESM1-0-LL	0.043 ± 0.005	0.063 ± 0.006	0.138 ± 0.006	0.098 ± 0.004	0.095 ± 0.005	0.158 ± 0.006

Table S8: The radiative forcing for total ozone calculated offline using the radiative kernel for *pdClim-2050ssp370fODS-radO3* minus *pdClim-control*. The results are separated for short wave clear sky (SW clear), short wave all sky (SW), long wave instantaneous clear sky (LW inst. clear), long wave instantaneous all sky (LW inst.), long wave including stratospheric temperature adjustments (LW. adj) and the net SARF (NET adj.). The uncertainty is the standard error calculated from the interannual variability. All values are in W m^{-2}.

	SW clear	SW	LW inst. clear	LW inst.	LW adj.	NET adj.
CESM2	0.022 ± 0.000	0.032 ± 0.000	0.104 ± 0.001	0.074 ± 0.000	0.114 ± 0.001	0.146 ± 0.001
EMAC	0.021 ± 0.000	0.030 ± 0.000	0.105 ± 0.001	0.074 ± 0.000	0.108 ± 0.001	0.138 ± 0.001
GFDL -ESM4	0.019 ± 0.000	0.028 ± 0.000	0.087 ± 0.001	0.061 ± 0.001	0.093 ± 0.001	0.121 ± 0.001
UKESM1.0 -LL	0.019 ± 0.001	0.027 ± 0.001	0.086 ± 0.002	0.060 ± 0.002	0.089 ± 0.003	0.116 ± 0.003

Table S9: The radiative forcing for tropospheric ozone calculated offline using the radiative kernel for *pdClim-2050ssp370fODS-radO3* minus *pdClim-control*. The results are separated for short wave clear sky (SW clear), short wave all sky (SW), long wave instantaneous clear sky (LW inst. clear), long wave instantaneous all sky (LW inst.), long wave including stratospheric temperature adjustments (LW. adj) and the net SARF (NET adj.). The uncertainty is the standard error calculated from the interannual variability. All values are in W m^{-2}.

	Cloud cover		(All-sky minus clear-sky) ERF		
	Reference [%]	Absolute Change [%]	SW ERF [W m^{-2}]	LW ERF [W m^{-2}]	Net ERF [W m^{-2}]
CESM2	69.12 ± 0.02	-0.08 ± 0.04	0.10 ± 0.05	-0.17 ± 0.03	-0.08 ± 0.05
EMAC	62.37 ± 0.11	-0.03 ± 0.01	0.05 ± 0.01	-0.09 ± 0.03	-0.04 ± 0.01
GFDL-ESM4	66.02 ± 0.02	-0.08 ± 0.03	0.10 ± 0.03	-0.14 ± 0.02	-0.04 ± 0.03
UKESM1-0-LL	69.14 ± 0.03	-0.20 ± 0.03	0.28 ± 0.03	-0.22 ± 0.02	0.05 ± 0.02
Multi-model mean	66.7 ± 2.8	-0.10 ± 0.06	0.13 ± 0.09	-0.16 ± 0.05	-0.02 ± 0.05
CESM2		-0.02 ± 0.04	-0.01 ± 0.05	-0.13 ± 0.02	-0.14 ± 0.05
EMAC		-0.01 ± 0.005	0.03 ± 0.01	-0.04 ± 0.01	-0.005 ± 0.005
GFDL-ESM4		-0.04 ± 0.03	-0.02 ± 0.03	-0.08 ± 0.01	-0.10 ± 0.03
UKESM1-0-LL		-0.10 ± 0.05	0.08 ± 0.03	-0.09 ± 0.02	-0.004 ± 0.02
Multi-model mean		-0.04 ± 0.03	0.02 ± 0.04	-0.08 ± 0.03	-0.06 ± 0.06

Table S10: Global mean cloud cover in reference simulation (*pdClim-control*), and absolute change in cloud cover and contribution of clouds to the SW, LW and net ERF for the *pdClim-2050ssp370-radO3* (top 4 rows) and *pdClim-2050ssp370fODS-radO3* (bottom 4 rows) experiments. The uncertainty for the individual models is the error on the mean, and the uncertainty on the multi-model mean is the standard deviation between the models.

	Surface albedo change	Albedo forcing [W m^{-2}]
CESM2	$-0.8\times10^{-4} \pm 0.7\times10^{-4}$	0.019 ± 0.017
EMAC	$-0.1\times10^{-4} \pm 0.03\times10^{-4}$	0.020 ± 0.001
GFDL-ESM4	$-1.3\times10^{-4} \pm 0.5\times10^{-4}$	0.031 ± 0.012
UKESM1-0-LL	$-0.6\times10^{-4} \pm 0.6\times10^{-4}$	0.014 ± 0.014
Multi-model mean	$-0.7\times10^{-4} \pm 0.4\times10^{-4}$	0.017 ± 0.010

Table S11: Global mean absolute surface albedo change and associated forcing from *pdClim-2050ssp370fODS-radO3* minus *pdClim-control*. Uncertainties for individual models are errors on the mean. Uncertainties for the multi-model mean are standard deviations across the models. Forcings are calculated using the formula in the text. Only models that provided surface SW fluxes are shown.

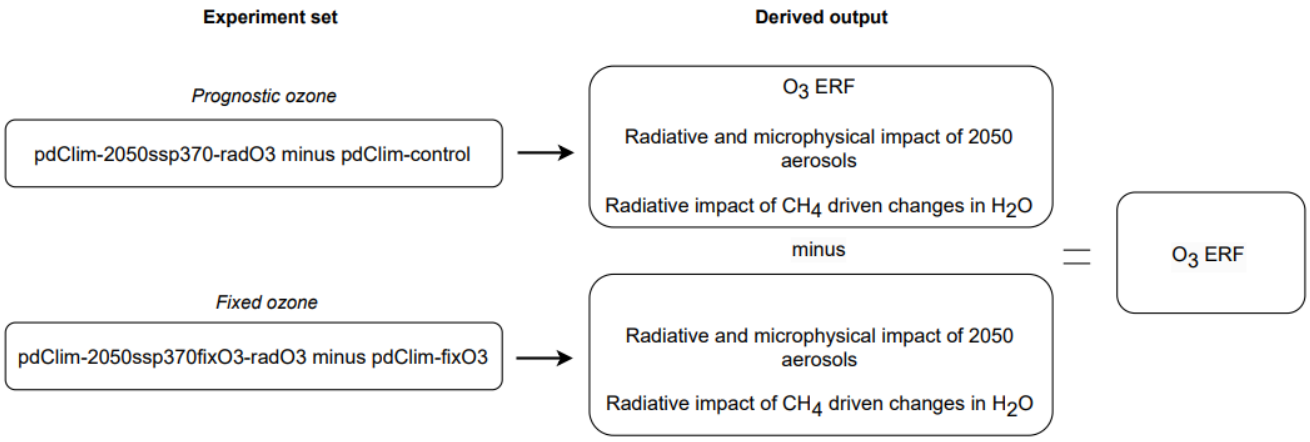

Figure S1: Schematic of the method to derive O_3 ERF with CESM2.

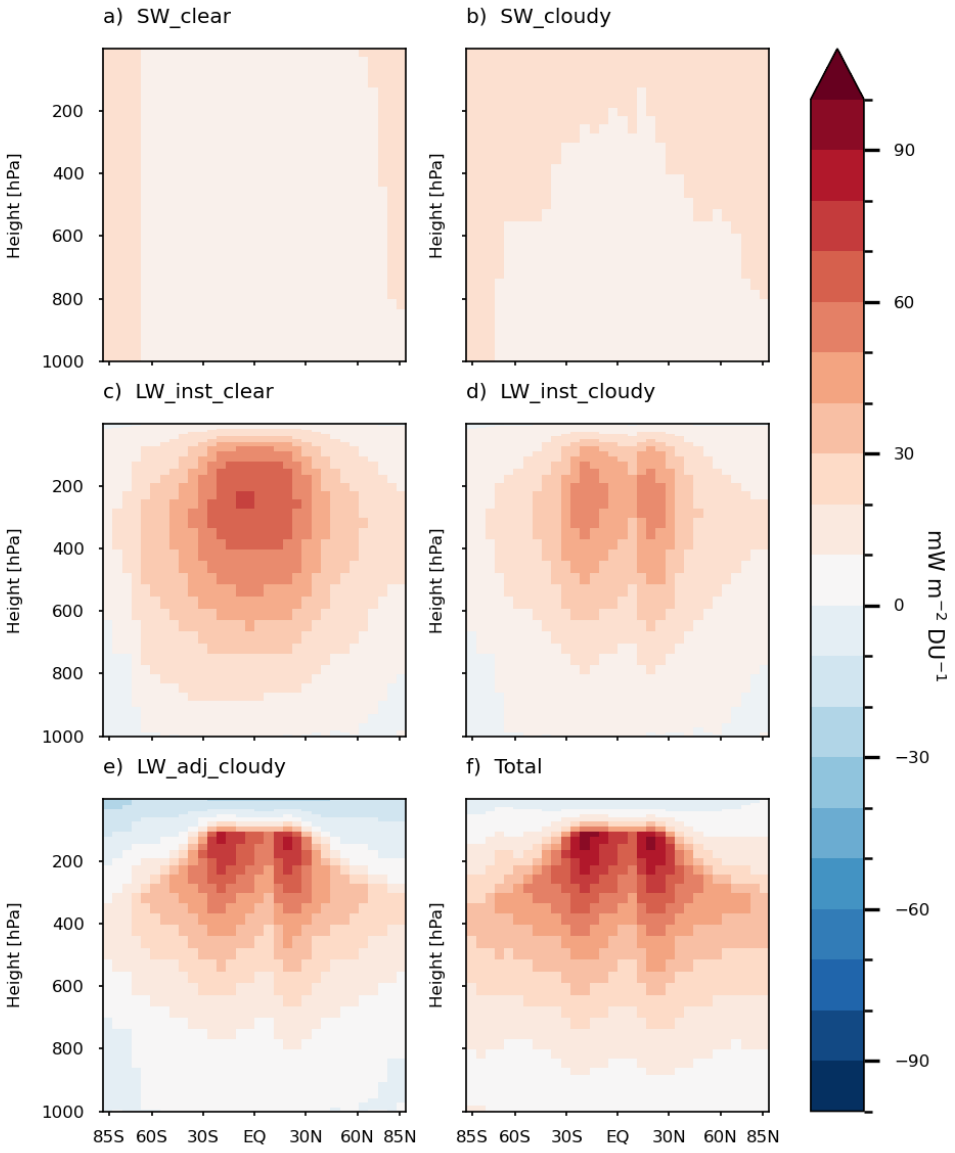

Figure S2: Annual zonal mean values of the TOA radiative kernel (mW m^{-2} per DU). In a) instantaneous radiative forcing (IRF) shortwave (SW) clear sky, b) IRF SW all sky, c) IRF longwave (LW) clear sky, d) IRF LW all sky, e) LW all sky with stratospheric adjustment and f) net forcing (LW all sky adjusted + SW all sky). The vertical coordinates are sigma hybrid-pressure levels and approximate pressure levels are used on the y-axis.

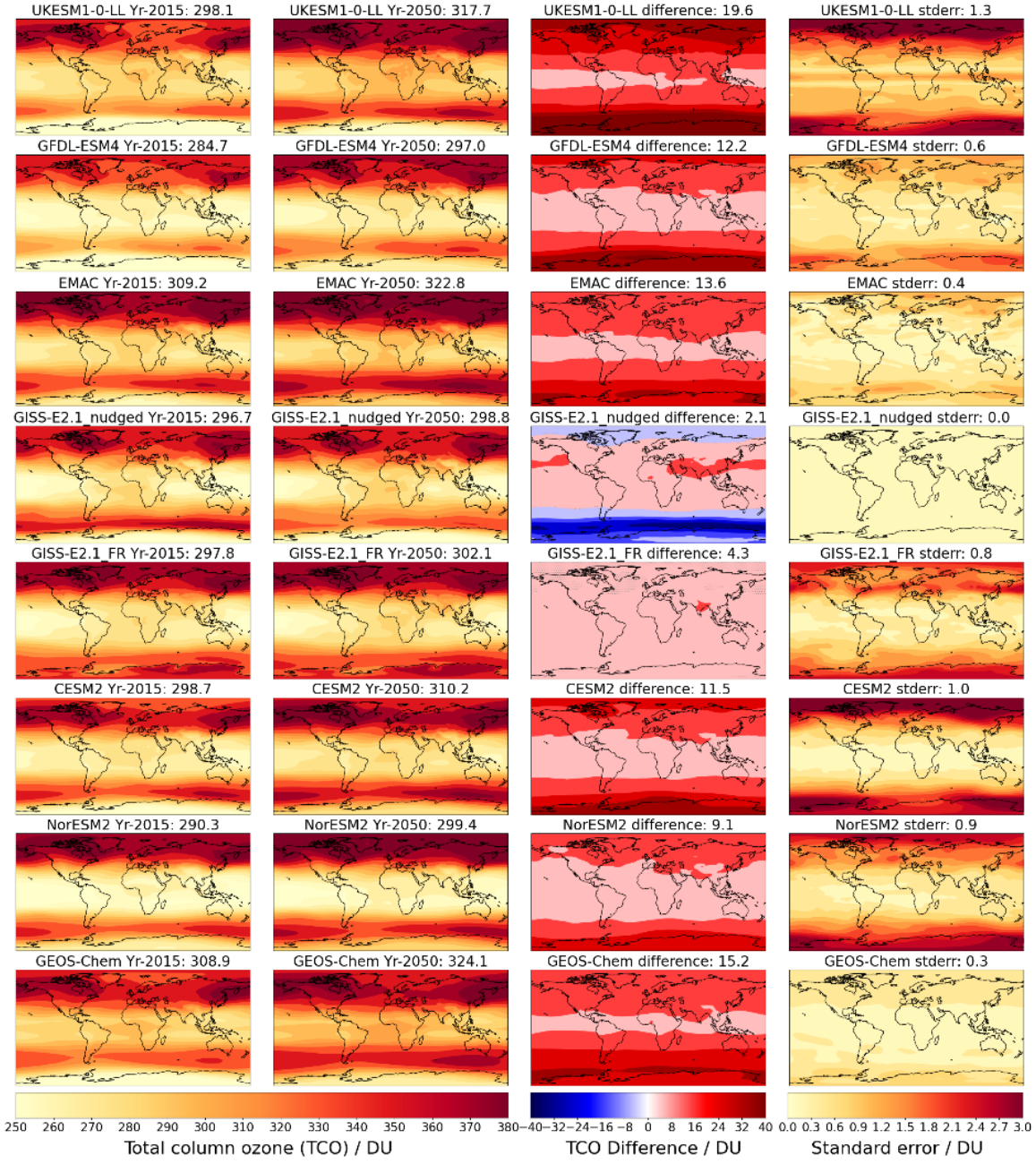

Figure S3: Year-2015 (1st column) and year-2050 (2nd column) climatologies for the global distribution of total column ozone (TCO), the difference between the two climatologies (3rd column; year-2050 minus year-2015), and the standard error in the difference (4th column) simulated by the models: UKESM1-0-LL, GFDL-ESM4, EMAC, GISS-E2.1_nudged, GISS-E2.1_FR, CESM2, NorESM2 and GEOS-Chem. The units for TCO are in Dobson Units (DU). Global mean values are shown above each panel.

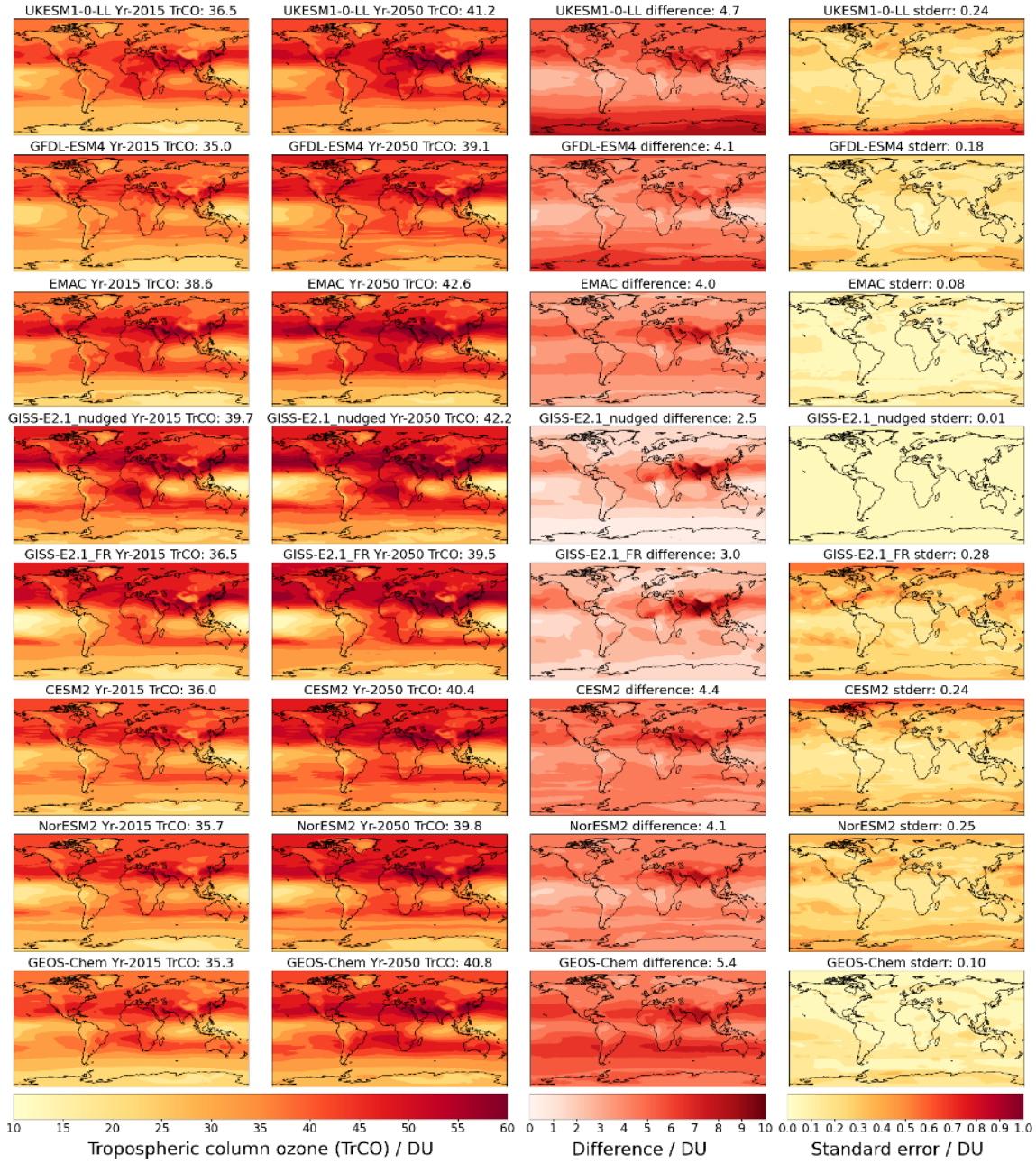

Figure S4: Year-2015 (1st column) and Year-2050 (2nd column) climatologies for the global distribution of tropospheric column ozone (TrCO), the difference between the two climatologies (3rd column; Year-2050 minus Year-2015), and the standard error in the difference (4th column) simulated by the models: UKESM1-0-LL, GFDL-ESM4, EMAC, GISS-E2.1_nudged, GISS-E2.1_FR, CESM2, NorESM2 and GEOS-Chem. The units for TrCO are in Dobson Units (DU).

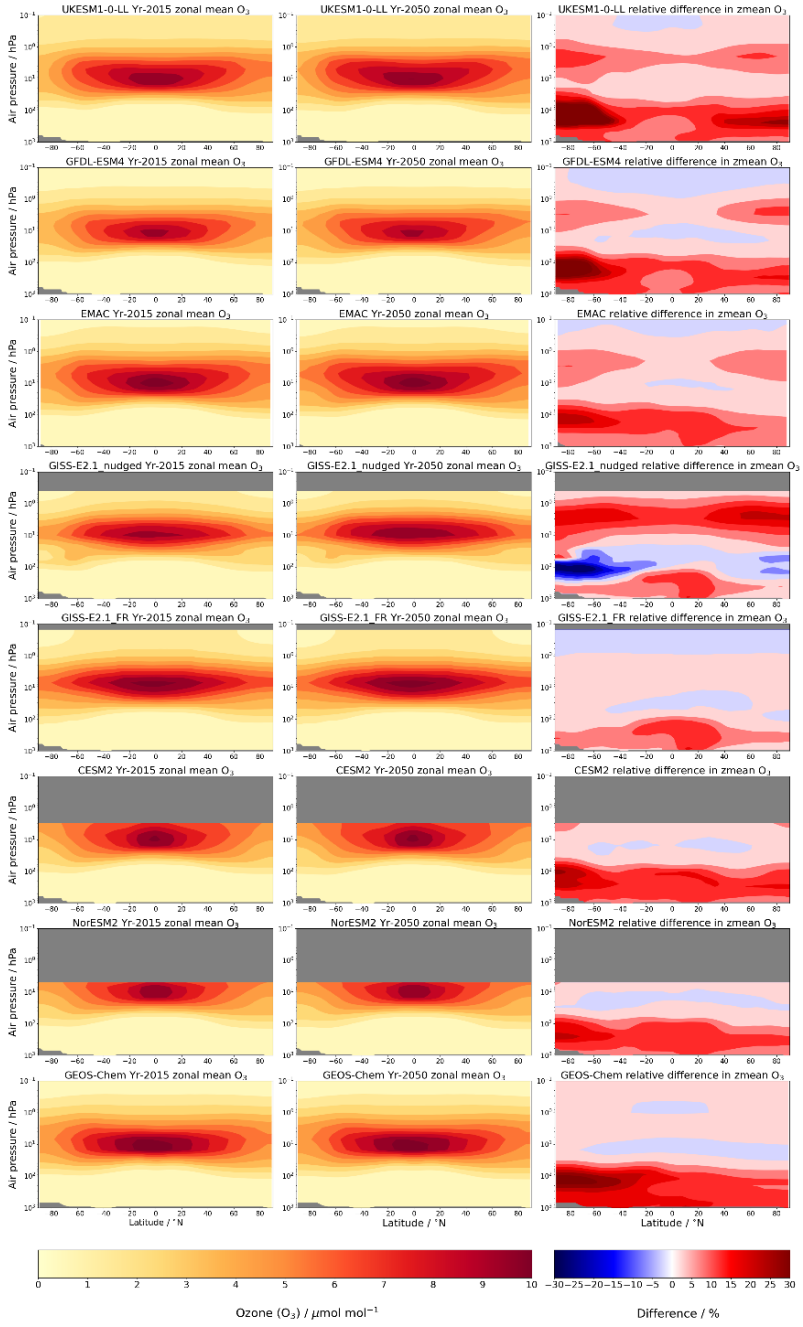

Figure S5: Year-2015 (1st column) and Year-2050 (2nd column) climatologies for the zonal mean distribution of ozone and the relative difference between the two climatologies (3rd column) from the TOAR simulations for the models: UKESM1-0-LL, GFDL-ESM4, EMAC, GISS-E2.1_nudged, GISS-E2.1_FR, CESM2, NorESM2 and GEOS-Chem. The units for ozone are in µmol mol^{-1} and the relative differences are in %. Pressure levels that are above the model top or pressure levels below the surface are greyed out.

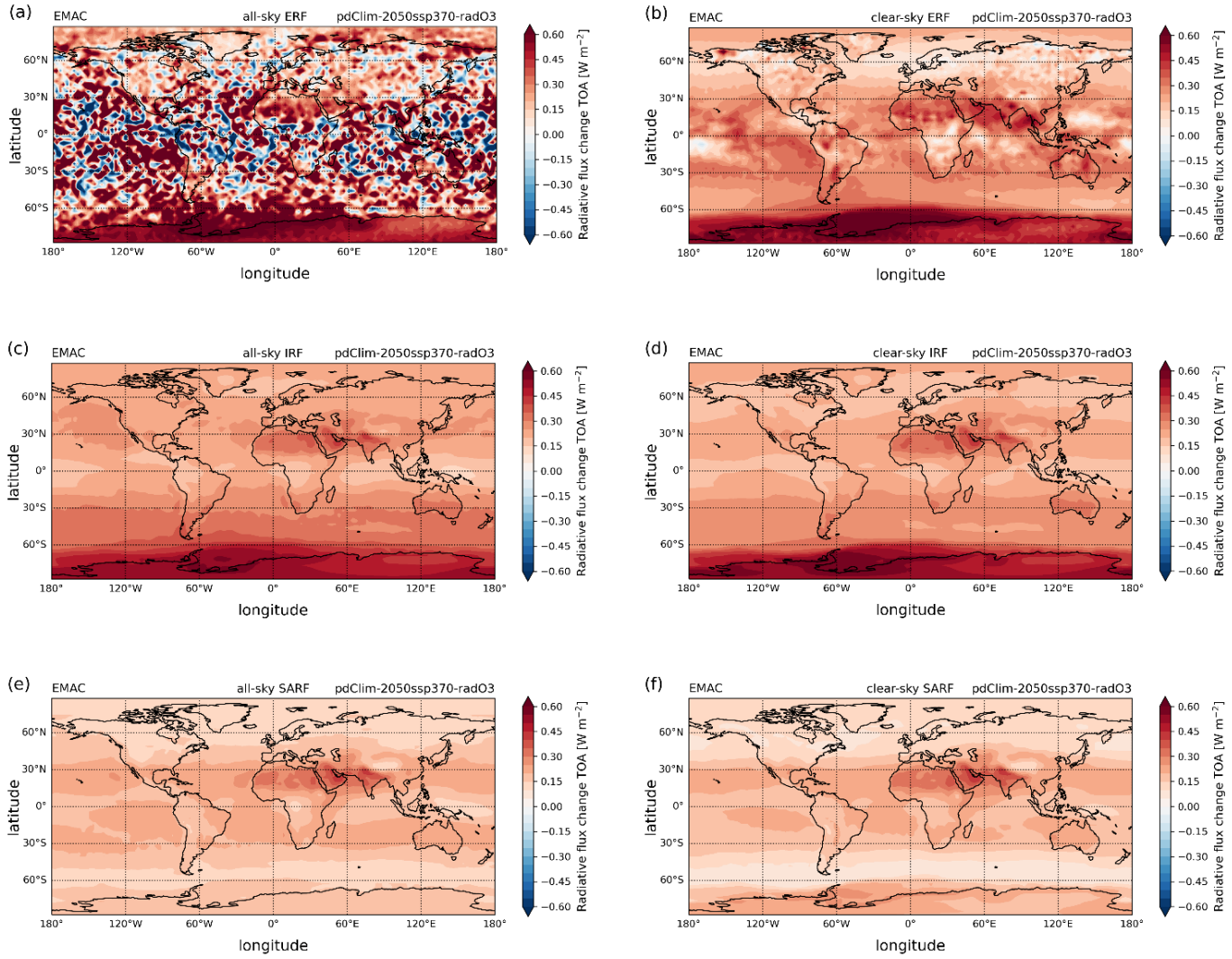

Figure S6: Spatial distribution of radiative flux changes from EMAC. Left column shows all-sky values for ERF (a), IRF (c) and SARF (e), whereas the right column shows the respective clear-sky values (b,d,f). ERF is calculated from pdClim-2050ssp370-radO3 minus pdClim-control. IRF and SARF are determined from multiple radiation call diagnostics in the EMAC pdClim-2050ssp370-radO3 simulation.

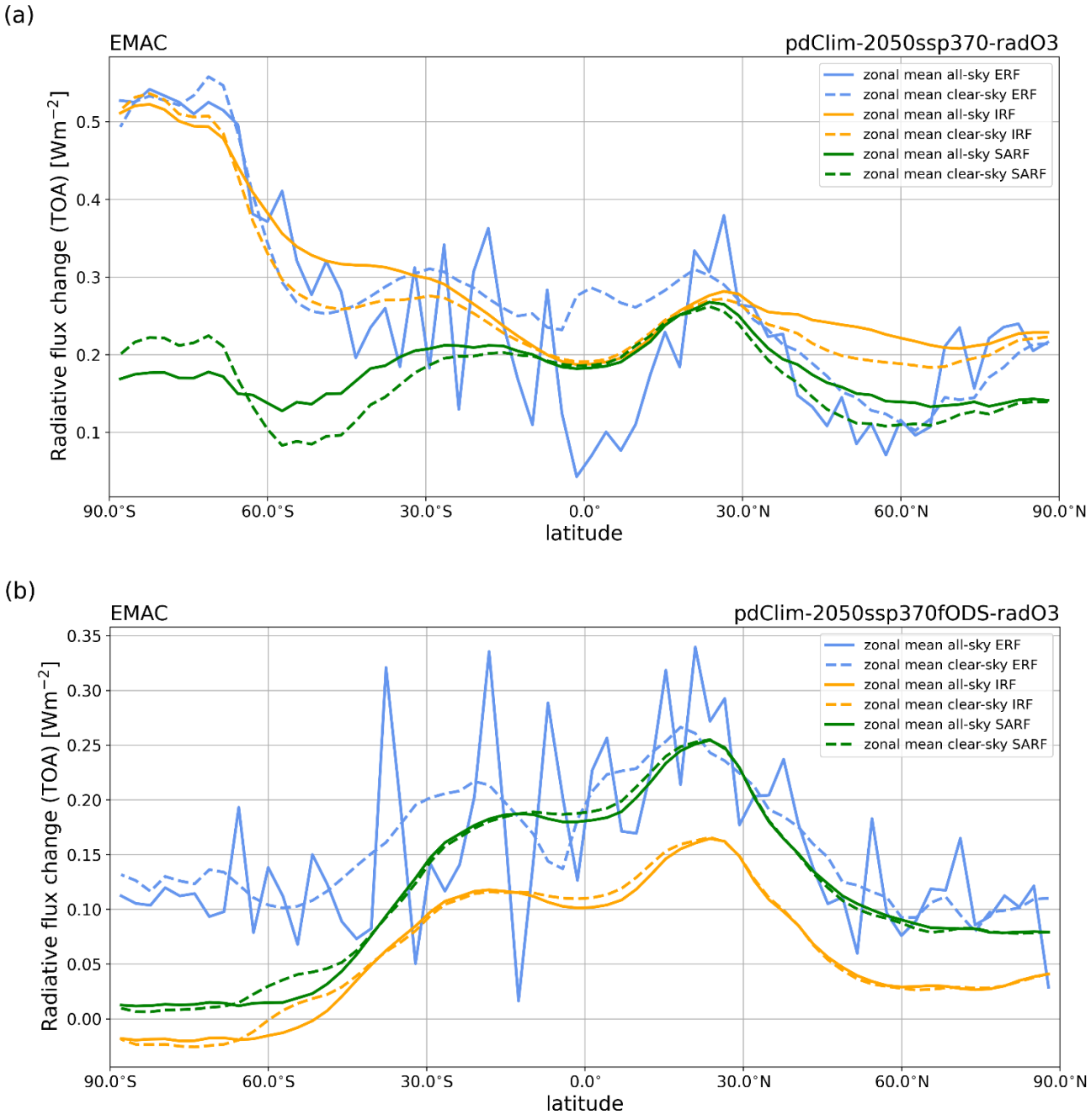

Figure S7: Zonal mean radiative flux changes for the EMAC pdClim-2050ssp370-radO3 simulation (a) and the EMAC pdClim-2050ssp370fODS-radO3 simulation (b). As in Fig. S6 the ERF values are calculated using the EMAC pdClim-control simulations, whereas IRF and SARF values are calculated using multiple radiation calls.

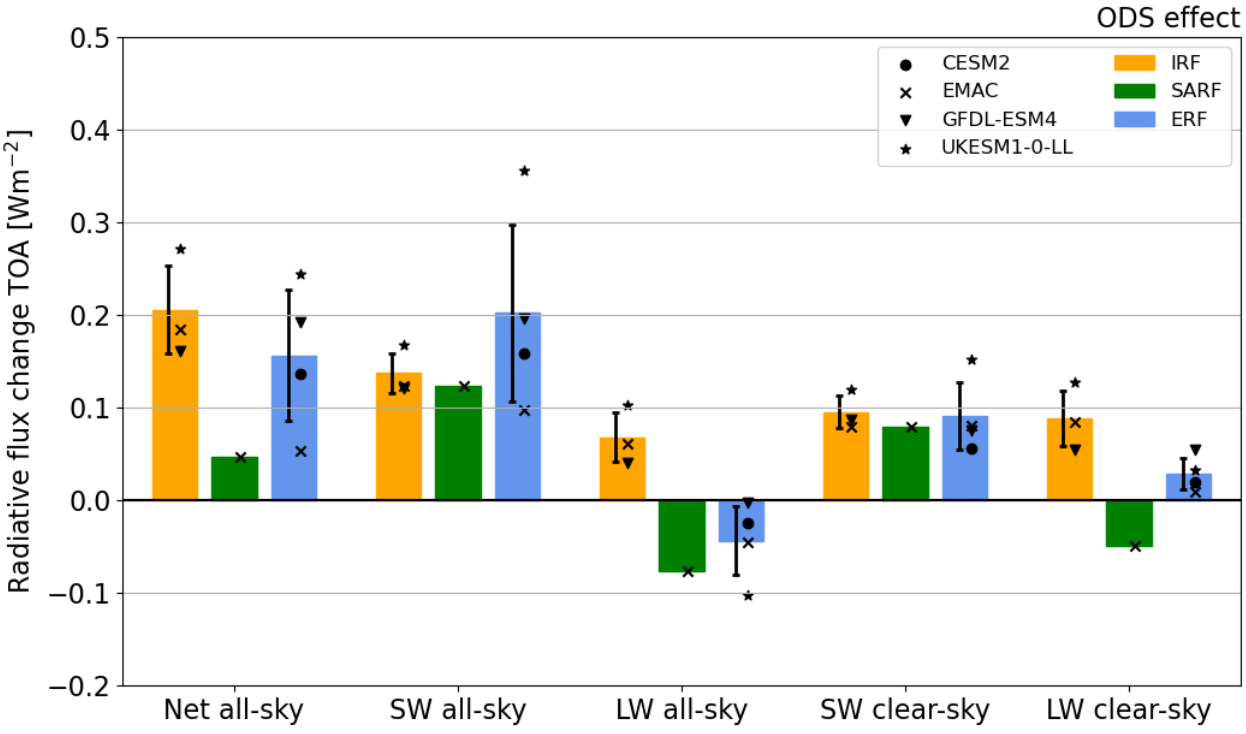

Figure S8: As Fig 7, but for the effect of ODS changes only.

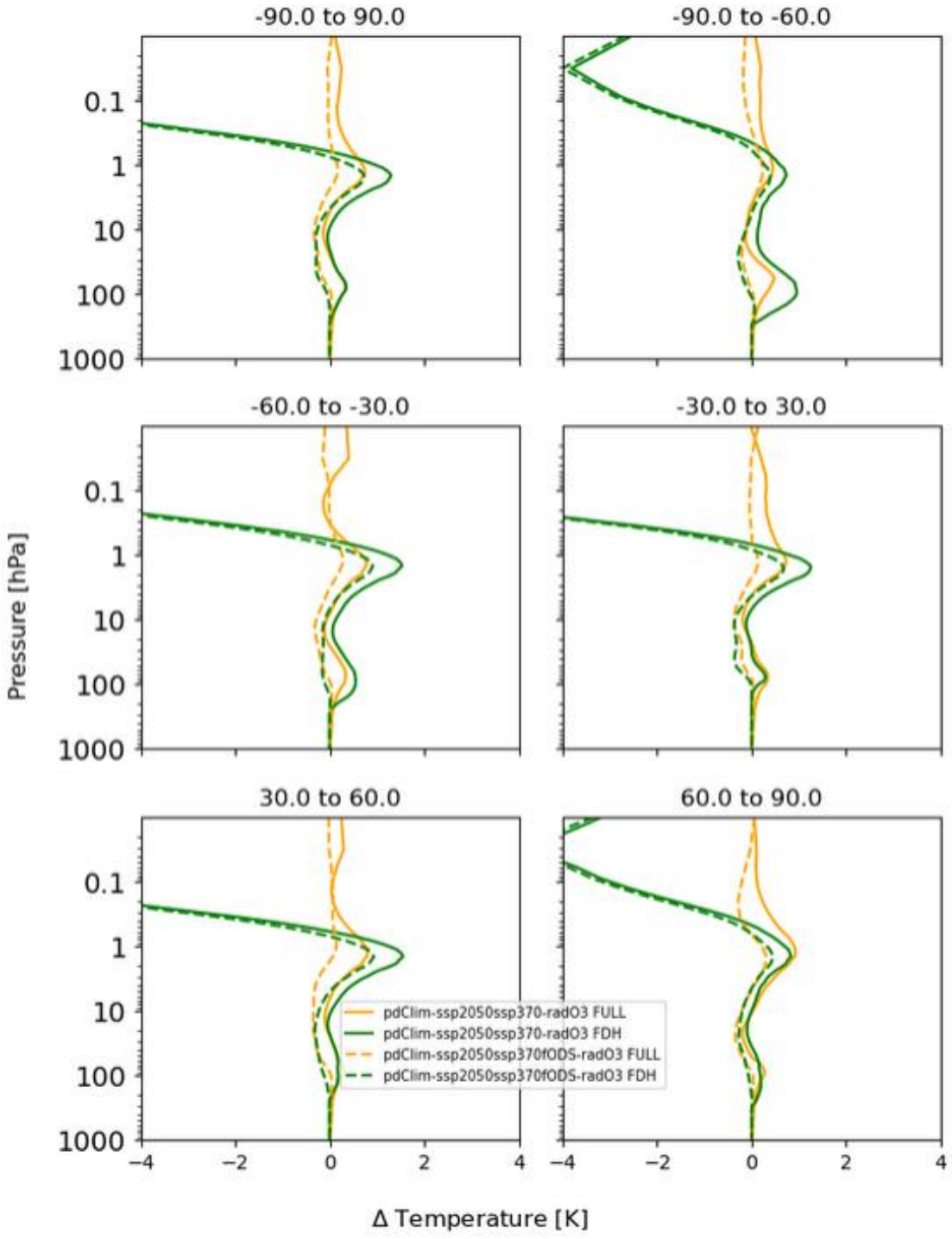

Figure S9: For the one model (EMAC) that calculated online SARF: Difference in temperature increments calculated by fixed-dynamical heating (FDH) in EMAC vs diagnosed from the ESM (FULL).

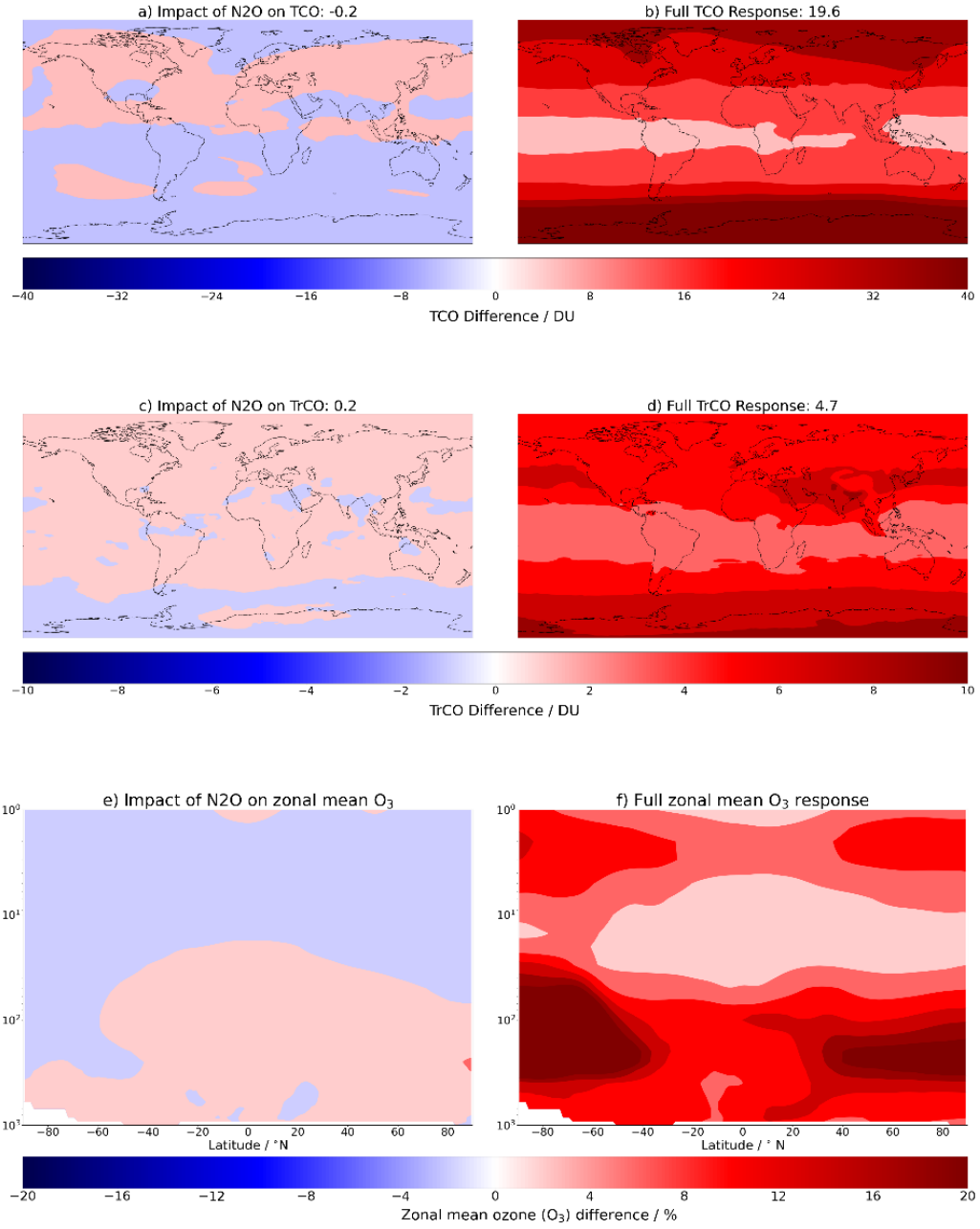

Figure S10: Differences in total column ozone (TCO), tropospheric column ozone (TrCO), and zonal mean ozone in 2050 relative to 2015 due to the increase in N2O following SSP3-7.0 in a), c), and e), respectively in comparison with the full ozone response on the right in b), d), and f) from UKESM1-0-LL.

References

Archibald, A. T., O'Connor, F. M., Abraham, N. L., Archer-Nicholls, S., Chipperfield, M. P., Dalvi, M., Folberth, G. A., Dennison, F., Dhomse, S. S., Griffiths, P. T., Hardacre, C., Hewitt, A. J., Hill, R. S., Johnson, C. E., Keeble, J., Köhler, M. O., Morgenstern, O., Mulcahy, J. P., Ordóñez, C., Pope, R. J., Rumbold, S. T., Russo, M. R., Savage, N. H., Sellar, A., Stringer, M., Turnock, S. T., Wild, O., and Zeng, G.: Description and evaluation of the UKCA stratosphere–troposphere chemistry scheme (StratTrop vn 1.0) implemented in UKESM1, Geosci Model Dev, 13, 1223–1266, https://doi.org/10.5194/gmd-13-1223-2020, 2020.

Bates, K. H., Evans, M. J., Henderson, B. H., and Jacob, D. J.: Impacts of updated reaction kinetics on the global GEOS-Chem simulation of atmospheric chemistry, Geosci Model Dev, 17, 1511–1524, https://doi.org/10.5194/gmd-17-1511-2024, 2024.

Bauer, S. E., Tsigaridis, K., Faluvegi, G., Kelley, M., Lo, K. K., Miller, R. L., Nazarenko, L., Schmidt, G. A., and Wu, J.: Historical (1850–2014) Aerosol Evolution and Role on Climate Forcing Using the GISS ModelE2.1 Contribution to CMIP6, J Adv Model Earth Syst, 12, e2019MS001978, https://doi.org/10.1029/2019MS001978, 2020.

Berntsen, T. K., Isaksen, I. S. A., Myhre, G., Fuglestvedt, J. S., Stordal, F., Alsvik Larsen, T., Freckleton, R. S., and Shine, K. P.: Effects of anthropogenic emissions on tropospheric ozone and its radiative forcing, Journal of Geophysical Research: Atmospheres, 102, 28101–28126, https://doi.org/10.1029/97JD02226, 1997.

Berntsen, T. K., Myhre, G., Stordal, F., and Isaksen, I. S. A.: Time evolution of tropospheric ozone and its radiative forcing, Journal of Geophysical Research Atmospheres, 105, 8915–8930, https://doi.org/10.1029/1999JD901139, 2000.

Brasseur, G. P., Kiehl, J. T., Müller, J. F., Schneider, T., Granier, C., Tie, X. X., and Hauglustaine, D.: Past and future changes in global tropospheric ozone: Impact on radiative forcing, Geophys Res Lett, 25, 3807–3810, https://doi.org/10.1029/1998GL900013, 1998.

Danabasoglu, G., Lamarque, J. F., Bacmeister, J., Bailey, D. A., DuVivier, A. K., Edwards, J., Emmons, L. K., Fasullo, J., Garcia, R., Gettelman, A., Hannay, C., Holland, M. M., Large, W. G., Lauritzen, P. H., Lawrence, D. M., Lenaerts, J. T. M., Lindsay, K., Lipscomb, W. H., Mills, M. J., Neale, R., Oleson, K. W., Otto-Bliesner, B., Phillips, A. S., Sacks, W., Tilmes, S., van Kampenhout, L., Vertenstein, M., Bertini, A., Dennis, J., Deser, C., Fischer, C., Fox-Kemper, B., Kay, J. E., Kinnison, D., Kushner, P. J., Larson, V. E., Long, M. C., Mickelson, S., Moore, J. K., Nienhouse, E., Polvani, L., Rasch, P. J., and Strand, W. G.: The Community Earth System Model Version 2 (CESM2), J Adv Model Earth Syst, 12, e2019MS001916, https://doi.org/10.1029/2019MS001916, 2020.

Dietmüller, S., Jöckel, P., Tost, H., Kunze, M., Gellhorn, C., Brinkop, S., Frömming, C., Ponater, M., Steil, B., Lauer, A., and Hendricks, J.: A new radiation infrastructure for the Modular Earth Submodel System (MESSy, based on version 2.51), Geosci Model Dev, 9, 2209–2222, https://doi.org/10.5194/gmd-9-2209-2016, 2016.

Van Dorland, R., Dentener, F. J., and Lelieveld, J.: Radiative forcing due to tropospheric ozone and sulfate aerosols, Journal of Geophysical Research: Atmospheres, 102, 28079–28100, https://doi.org/10.1029/97JD02499, 1997.

Dunne, J. P., Horowitz, L. W., Adcroft, A. J., Ginoux, P., Held, I. M., John, J. G., Krasting, J. P., Malyshev, S., Naik, V., Paulot, F., Shevliakova, E., Stock, C. A., Zadeh, N., Balaji, V., Blanton, C., Dunne, K. A., Dupuis, C., Durachta, J., Dussin,

R., Gauthier, P. P. G., Griffies, S. M., Guo, H., Hallberg, R. W., Harrison, M., He, J., Hurlin, W., McHugh, C., Menzel, R., Milly, P. C. D., Nikonov, S., Paynter, D. J., Ploshay, J., Radhakrishnan, A., Rand, K., Reichl, B. G., Robinson, T., Schwarzkopf, D. M., Sentman, L. T., Underwood, S., Vahlenkamp, H., Winton, M., Wittenberg, A. T., Wyman, B., Zeng, Y., and Zhao, M.: The GFDL Earth System Model Version 4.1 (GFDL-ESM 4.1): Overall Coupled Model Description and Simulation Characteristics, J Adv Model Earth Syst, 12, e2019MS002015, https://doi.org/10.1029/2019MS002015, 2020.

Emmons, L. K., Schwantes, R. H., Orlando, J. J., Tyndall, G., Kinnison, D., Lamarque, J. F., Marsh, D., Mills, M. J., Tilmes, S., Bardeen, C., Buchholz, R. R., Conley, A., Gettelman, A., Garcia, R., Simpson, I., Blake, D. R., Meinardi, S., and Pétron, G.: The Chemistry Mechanism in the Community Earth System Model Version 2 (CESM2), J Adv Model Earth Syst, 12, e2019MS001882, https://doi.org/10.1029/2019MS001882, 2020.

Eyring, V., Bony, S., Meehl, G. A., Senior, C. A., Stevens, B., Stouffer, R. J., and Taylor, K. E.: Overview of the Coupled Model Intercomparison Project Phase 6 (CMIP6) experimental design and organization, Geosci Model Dev, 9, 1937–1958, https://doi.org/10.5194/gmd-9-1937-2016, 2016.

Fouquart, Y. and Bonnel, B.: Computations of solar heating of the earth's atmosphere: A new parameterization, Beitr. Phys. Atmos., 53, 35–62, 1980.

Gauss, M., Myhre, G., Isaksen, I. S. A., Grewe, V., Pitari, G., Wild, O., Collins, W. J., Dentener, F. J., Ellingsen, K., Gohar, L. K., Hauglustaine, D. A., Iachetti, D., Lamarque, F., Mancini, E., Mickley, L. J., Prather, M. J., Pyle, J. A., Sanderson, M. G., Shine, K. P., Stevenson, D. S., Sudo, K., Szopa, S., and Zeng, G.: Radiative forcing since preindustrial times due to ozone change in the troposphere and the lower stratosphere, Atmos Chem Phys, 6, 575–599, https://doi.org/10.5194/acp-6-575-2006, 2006.

Gery, M. W., Whitten, G. Z., Killus, J. P., and Dodge, M. C.: A photochemical kinetics mechanism for urban and regional scale computer modeling, Journal of Geophysical Research: Atmospheres, 94, 12925–12956, https://doi.org/10.1029/JD094ID10P12925, 1989.

Guenther, A. B., Jiang, X., Heald, C. L., Sakulyanontvittaya, T., Duhl, T., Emmons, L. K., and Wang, X.: The Model of Emissions of Gases and Aerosols from Nature version 2.1 (MEGAN2.1): an extended and updated framework for modeling biogenic emissions, Geosci Model Dev, 5, 1471–1492, https://doi.org/10.5194/gmd-5-1471-2012, 2012.

Harris, L. M. and Lin, S. J.: A Two-Way Nested Global-Regional Dynamical Core on the Cubed-Sphere Grid, Mon Weather Rev, 141, 283–306, https://doi.org/10.1175/MWR-D-11-00201.1, 2013.

Hauglustaine, D. A. and Brasseur, G. P.: Evolution of tropospheric ozone under anthropogenic activities and associated radiative forcing of climate, Journal of Geophysical Research: Atmospheres, 106, 32337–32360, https://doi.org/10.1029/2001JD900175, 2001.

Hauglustaine, D. A., Granier, C., Brasseur, G. P., and Mégie, G.: The importance of atmospheric chemistry in the calculation of radiative forcing on the climate system, Journal of Geophysical Research: Atmospheres, 99, 1173–1186, https://doi.org/10.1029/93JD02987, 1994.

Haywood, J. M., Schwarzkopf, M. D., and Ramaswamy, V.: Estimates of radiative forcing due to modeled increases in tropospheric ozone, Journal of Geophysical Research: Atmospheres, 103, 16999–17007, https://doi.org/10.1029/98JD01348, 1998.

Heald, C. L., Ridley, D. A., Kroll, J. H., Barrett, S. R. H., Cady-Pereira, K. E., Alvarado, M. J., and Holmes, C. D.: Contrasting the direct radiative effect and direct radiative forcing of aerosols, Atmos Chem Phys, 14, 5513–5527, https://doi.org/10.5194/acp-14-5513-2014, 2014.

Horowitz, L. W., Naik, V., Paulot, F., Ginoux, P. A., Dunne, J. P., Mao, J., Schnell, J., Chen, X., He, J., John, J. G., Lin, M., Lin, P., Malyshev, S., Paynter, D., Shevliakova, E., and Zhao, M.: The GFDL Global Atmospheric Chemistry-Climate Model AM4.1: Model Description and Simulation Characteristics, J Adv Model Earth Syst, 12, e2019MS002032, https://doi.org/10.1029/2019MS002032, 2020.

Hu, L., Millet, D. B., Baasandorj, M., Griffis, T. J., Turner, P., Helmig, D., Curtis, A. J., and Hueber, J.: Isoprene emissions and impacts over an ecological transition region in the U.S. Upper Midwest inferred from tall tower measurements, Journal of Geophysical Research: Atmospheres, 120, 3553–3571, https://doi.org/10.1002/2014JD022732, 2015.

Hudman, R. C., Moore, N. E., Mebust, A. K., Martin, R. V., Russell, A. R., Valin, L. C., and Cohen, R. C.: Steps towards a mechanistic model of global soil nitric oxide emissions: implementation and space based-constraints, Atmos Chem Phys, 12, 7779–7795, https://doi.org/10.5194/acp-12-7779-2012, 2012.

Iacono, M. J., Delamere, J. S., Mlawer, E. J., Shephard, M. W., Clough, S. A., and Collins, W. D.: Radiative forcing by long-lived greenhouse gases: Calculations with the AER radiative transfer models, Journal of Geophysical Research: Atmospheres, 113, 13103, https://doi.org/10.1029/2008JD009944, 2008.

Jöckel, P., Kerkweg, A., Pozzer, A., Sander, R., Tost, H., Riede, H., Baumgaertner, A., Gromov, S., and Kern, B.: Development cycle 2 of the Modular Earth Submodel System (MESSy2), Geosci Model Dev, 3, 717–752, https://doi.org/10.5194/gmd-3-717-2010, 2010.

Jöckel, P., Tost, H., Pozzer, A., Kunze, M., Kirner, O., Brenninkmeijer, C. A. M., Brinkop, S., Cai, D. S., Dyroff, C., Eckstein, J., Frank, F., Garny, H., Gottschaldt, K.-D., Graf, P., Grewe, V., Kerkweg, A., Kern, B., Matthes, S., Mertens, M., Meul, S., Neumaier, M., Nützel, M., Oberländer-Hayn, S., Ruhnke, R., Runde, T., Sander, R., Scharffe, D., and Zahn, A.: Earth System Chemistry integrated Modelling (ESCiMo) with the Modular Earth Submodel System (MESSy) version 2.51, Geosci Model Dev, 9, 1153–1200, https://doi.org/10.5194/gmd-9-1153-2016, 2016.

Keeble, J., Hassler, B., Banerjee, A., Checa-Garcia, R., Chiodo, G., Davis, S., Eyring, V., Griffiths, P. T., Morgenstern, O., Nowack, P., Zeng, G., Zhang, J., Bodeker, G., Burrows, S., Cameron-Smith, P., Cugnet, D., Danek, C., Deushi, M., Horowitz, L. W., Kubin, A., Li, L., Lohmann, G., Michou, M., Mills, M. J., Nabat, P., Olivié, D., Park, S., Seland, Ø., Stoll, J., Wieners, K. H., and Wu, T.: Evaluating stratospheric ozone and water vapour changes in CMIP6 models from 1850 to 2100, Atmos Chem Phys, 21, 5015–5061, https://doi.org/10.5194/ACP-21-5015-2021, 2021.

Kelley, M., Schmidt, G. A., Nazarenko, L. S., Bauer, S. E., Ruedy, R., Russell, G. L., Ackerman, A. S., Aleinov, I., Bauer, M., Bleck, R., Canuto, V., Cesana, G., Cheng, Y., Clune, T. L., Cook, B. I., Cruz, C. A., Del Genio, A. D., Elsaesser, G. S., Faluvegi, G., Kiang, N. Y., Kim, D., Lacis, A. A., Leboissetier, A., LeGrande, A. N., Lo, K. K., Marshall, J., Matthews, E. E., McDermid, S., Mezuman, K., Miller, R. L., Murray, L. T., Oinas, V., Orbe, C., García-Pando, C. P., Perlwitz, J. P., Puma, M. J., Rind, D., Romanou, A., Shindell, D. T., Sun, S., Tausnev, N., Tsigaridis, K., Tselioudis, G., Weng, E., Wu, J., and Yao, M. S.: GISS-E2.1: Configurations and Climatology, J Adv Model Earth Syst, 12, e2019MS002025, https://doi.org/10.1029/2019MS002025, 2020.

Kiehl, J. T., Schneider, T. L., Portmann, R. W., and Solomon, S.: Climate forcing due to tropospheric and stratospheric ozone, Journal of Geophysical Research Atmospheres, 104, 31239–31254, https://doi.org/10.1029/1999JD900991, 1999.

Kirkevåg, A., Grini, A., Olivié, D., Seland, Ø., Alterskjær, K., Hummel, M., Karset, I. H. H., Lewinschal, A., Liu, X., Makkonen, R., Bethke, I., Griesfeller, J., Schulz, M., and Iversen, T.: A production-tagged aerosol module for Earth system models, OsloAero5.3 – extensions and updates for CAM5.3-Oslo, Geosci Model Dev, 11, 3945–3982, https://doi.org/10.5194/gmd-11-3945-2018, 2018.

Kirner, O., Ruhnke, R., Buchholz-Dietsch, J., Jöckel, P., Brühl, C., and Steil, B.: Simulation of polar stratospheric clouds in the chemistry-climate-model EMAC via the submodel PSC, Geosci Model Dev, 4, 169–182, https://doi.org/10.5194/gmd-4-169-2011, 2011.

Kunze, M., Godolt, M., Langematz, U., Grenfell, J. L., Hamann-Reinus, A., and Rauer, H.: Investigating the early Earth faint young Sun problem with a general circulation model, Planet Space Sci, 98, 77–92, https://doi.org/10.1016/J.PSS.2013.09.011, 2014.

Lacis, A. A. and Oinas, V.: A description of the correlated k distribution method for modeling nongray gaseous absorption, thermal emission, and multiple scattering in vertically inhomogeneous atmospheres, Journal of Geophysical Research: Atmospheres, 96, 9027–9063, https://doi.org/10.1029/90JD01945, 1991.

Lelieveld, J. and Dentener, F. J.: What controls tropospheric ozone?, Journal of Geophysical Research: Atmospheres, 105, 3531–3551, https://doi.org/10.1029/1999JD901011, 2000.

Liao, H. and Seinfeld, J. H.: Global impacts of gas-phase chemistry-aerosol interactions on direct radiative forcing by anthropogenic aerosols and ozone, Journal of Geophysical Research: Atmospheres, 110, 1–22, https://doi.org/10.1029/2005JD005907, 2005.

Liu, X., Ma, P.-L., Wang, H., Tilmes, S., Singh, B., Easter, R. C., Ghan, S. J., and Rasch, P. J.: Description and evaluation of a new four-mode version of the Modal Aerosol Module (MAM4) within version 5.3 of the Community Atmosphere Model, Geosci Model Dev, 9, 505–522, https://doi.org/10.5194/gmd-9-505-2016, 2016.

Mickley, L. J., Jacob, D. J., and Rind, D.: Uncertainty in preindustrial abundance of tropospheric ozone: Implications for radiative forcing calculations, Journal of Geophysical Research Atmospheres, 106, 3389–3399, https://doi.org/10.1029/2000JD900594, 2001.

Mickley, L. J., Jacob, D. J., Field, B. D., and Rind, D.: Climate response to the increase in tropospheric ozone since preindustrial times: A comparison between ozone and equivalent CO2 forcings, Journal of Geophysical Research: Atmospheres, 109, 5106, https://doi.org/10.1029/2003JD003653, 2004.

Miller, R. L., Schmidt, G. A., Nazarenko, L. S., Bauer, S. E., Kelley, M., Ruedy, R., Russell, G. L., Ackerman, A. S., Aleinov, I., Bauer, M., Bleck, R., Canuto, V., Cesana, G., Cheng, Y., Clune, T. L., Cook, B. I., Cruz, C. A., Del Genio, A. D., Elsaesser, G. S., Faluvegi, G., Kiang, N. Y., Kim, D., Lacis, A. A., Leboissetier, A., LeGrande, A. N., Lo, K. K., Marshall, J., Matthews, E. E., McDermid, S., Mezuman, K., Murray, L. T., Oinas, V., Orbe, C., Pérez García-Pando, C., Perlwitz, J. P., Puma, M. J., Rind, D., Romanou, A., Shindell, D. T., Sun, S., Tausnev, N., Tsigaridis, K., Tselioudis, G., Weng, E., Wu, J., and Yao, M. S.: CMIP6 Historical Simulations (1850–2014) With GISS-E2.1, J Adv Model Earth Syst, 13, e2019MS002034, https://doi.org/10.1029/2019MS002034, 2021.

Morgenstern, O., Braesicke, P., O'Connor, F. M., Bushell, A. C., Johnson, C. E., Osprey, S. M., and Pyle, J. A.: Evaluation of the new UKCA climate-composition model – Part 1: The stratosphere, Geosci Model Dev, 2, 43–57, https://doi.org/10.5194/gmd-2-43-2009, 2009.

Morgenstern, O., O'Connor, F. M., Johnson, B. T., Zeng, G., Mulcahy, J. P., Williams, J., Teixeira, J., Michou, M., Nabat, P., Horowitz, L. W., Naik, V., Sentman, L. T., Deushi, M., Bauer, S. E., Tsigaridis, K., Shindell, D. T., and Kinnison, D. E.: Reappraisal of the Climate Impacts of Ozone-Depleting Substances, Geophys Res Lett, 47, e2020GL088295, https://doi.org/10.1029/2020GL088295, 2020.

Murray, L. T., Jacob, D. J., Logan, J. A., Hudman, R. C., Koshak, W. J., Murray, L. T., Jacob, D. J., Logan, J. A., Hudman, R. C., and Koshak, W. J.: Optimized regional and interannual variability of lightning in a global chemical transport model constrained by LIS/OTD satellite data, Journal of Geophysical Research: Atmospheres, 117, 20307, https://doi.org/10.1029/2012JD017934, 2012.

Nazarenko, L. S., Tausnev, N., Russell, G. L., Rind, D., Miller, R. L., Schmidt, G. A., Bauer, S. E., Kelley, M., Ruedy, R., Ackerman, A. S., Aleinov, I., Bauer, M., Bleck, R., Canuto, V., Cesana, G., Cheng, Y., Clune, T. L., Cook, B. I., Cruz, C. A., Del Genio, A. D., Elsaesser, G. S., Faluvegi, G., Kiang, N. Y., Kim, D., Lacis, A. A., Leboissetier, A., LeGrande, A. N., Lo, K. K., Marshall, J., Matthews, E. E., McDermid, S., Mezuman, K., Murray, L. T., Oinas, V., Orbe, C., García-Pando, C. P., Perlwitz, J. P., Puma, M. J., Romanou, A., Shindell, D. T., Sun, S., Tsigaridis, K., Tselioudis, G., Weng, E., Wu, J., and Yao, M. S.: Future Climate Change Under SSP Emission Scenarios With GISS-E2.1, J Adv Model Earth Syst, 14, e2021MS002871, https://doi.org/10.1029/2021MS002871, 2022.

Nützel, M., Stecher, L., Jöckel, P., Winterstein, F., Dameris, M., Ponater, M., Graf, P., and Kunze, M.: Updating the radiation infrastructure in MESSy (based on MESSy version 2.55), Geosci Model Dev, 17, 5821–5849, https://doi.org/10.5194/GMD-17-5821-2024, 2024.

O'Connor, F. M., Johnson, C. E., Morgenstern, O., Abraham, N. L., Braesicke, P., Dalvi, M., Folberth, G. A., Sanderson, M. G., Telford, P. J., Voulgarakis, A., Young, P. J., Zeng, G., Collins, W. J., and Pyle, J. A.: Evaluation of the new UKCA climate-composition model – Part 2: The Troposphere, Geosci Model Dev, 7, 41–91, https://doi.org/10.5194/gmd-7-41-2014, 2014.

Pöschl, U., Von Kuhlmann, R., Poisson, N., and Crutzen, P. J.: Development and intercomparison of condensed isoprene oxidation mechanisms for global atmospheric modeling, J Atmos Chem, 37, 29–52, https://doi.org/10.1023/A:1006391009798, 2000.

Putman, W. M. and Lin, S. J.: Finite-volume transport on various cubed-sphere grids, J Comput Phys, 227, 55–78, https://doi.org/10.1016/J.JCP.2007.07.022, 2007.

Rivera, A., Tsigaridis, K., Faluvegi, G., and Shindell, D.: Assessing acetone for the GISS ModelE2.1 Earth system model, Geosci Model Dev, 17, 3487–3505, https://doi.org/10.5194/GMD-17-3487-2024, 2024.

Roeckner, E., Brokopf, R., Esch, M., Giorgetta, M. A., Hagemann, S., Kornblueh, L., Manzini, E., Schlese, U., and Schulzweida, U.: Sensitivity of Simulated Climate to Horizontal and Vertical Resolution in the ECHAM5 Atmosphere Model, J Clim, 19, 3771–3791, https://doi.org/10.1175/JCLI3824.1, 2006.

Roelofs, G. J., Lelieveld, J., and Van Dorland, R.: A three-dimensional chemistry/general circulation model simulation of anthropogenically derived ozone in the troposphere and its radiative climate forcing, Journal of Geophysical Research: Atmospheres, 102, 23389–23401, https://doi.org/10.1029/97JD02210, 1997.

Sander, R., Baumgaertner, A., Cabrera-Perez, D., Frank, F., Gromov, S., Grooß, J.-U., Harder, H., Huijnen, V., Jöckel, P., Karydis, V. A., Niemeyer, K. E., Pozzer, A., Riede, H., Schultz, M. G., Taraborrelli, D., and Tauer, S.: The community

atmospheric chemistry box model CAABA/MECCA-4.0, Geosci Model Dev, 12, 1365–1385, https://doi.org/10.5194/gmd-12-1365-2019, 2019.

Seland, Ø., Bentsen, M., Olivié, D., Toniazzo, T., Gjermundsen, A., Graff, L. S., Debernard, J. B., Gupta, A. K., He, Y.-C., Kirkevåg, A., Schwinger, J., Tjiputra, J., Aas, K. S., Bethke, I., Fan, Y., Griesfeller, J., Grini, A., Guo, C., Ilicak, M., Karset, I. H. H., Landgren, O., Liakka, J., Moseid, K. O., Nummelin, A., Spensberger, C., Tang, H., Zhang, Z., Heinze, C., Iversen, T., and Schulz, M.: Overview of the Norwegian Earth System Model (NorESM2) and key climate response of CMIP6 DECK, historical, and scenario simulations, Geosci Model Dev, 13, 6165–6200, https://doi.org/10.5194/gmd-13-6165-2020, 2020.

Sellar, A. A., Jones, C. G., Mulcahy, J. P., Tang, Y., Yool, A., Wiltshire, A., O'Connor, F. M., Stringer, M., Hill, R., Palmieri, J., Woodward, S., de Mora, L., Kuhlbrodt, T., Rumbold, S. T., Kelley, D. I., Ellis, R., Johnson, C. E., Walton, J., Abraham, N. L., Andrews, M. B., Andrews, T., Archibald, A. T., Berthou, S., Burke, E., Blockley, E., Carslaw, K., Dalvi, M., Edwards, J., Folberth, G. A., Gedney, N., Griffiths, P. T., Harper, A. B., Hendry, M. A., Hewitt, A. J., Johnson, B., Jones, A., Jones, C. D., Keeble, J., Liddicoat, S., Morgenstern, O., Parker, R. J., Predoi, V., Robertson, E., Siahaan, A., Smith, R. S., Swaminathan, R., Woodhouse, M. T., Zeng, G., and Zerroukat, M.: UKESM1: Description and Evaluation of the U.K. Earth System Model, J Adv Model Earth Syst, 11, 4513–4558, https://doi.org/10.1029/2019MS001739, 2019.

Shevliakova, E., Malyshev, S., Martinez-Cano, I., Milly, P. C. D., Pacala, S. W., Ginoux, P., Dunne, K. A., Dunne, J. P., Dupuis, C., Findell, K. L., Ghannam, K., Horowitz, L. W., Knutson, T. R., Krasting, J. P., Naik, V., Phillipps, P., Zadeh, N., Yu, Y., Zeng, F., and Zeng, Y.: The Land Component LM4.1 of the GFDL Earth System Model ESM4.1: Model Description and Characteristics of Land Surface Climate and Carbon Cycling in the Historical Simulation, J Adv Model Earth Syst, 16, e2023MS003922, https://doi.org/10.1029/2023MS003922, 2024.

Shindell, D. T., Grenfell, J. L., Rind, D., Grewe, V., and Price, C.: Chemistry-climate interactions in the Goddard Institute for Space Studies general circulation model: 1. Tropospheric chemistry model description and evaluation, Journal of Geophysical Research: Atmospheres, 106, 8047–8075, https://doi.org/10.1029/2000JD900704, 2001.

Shindell, D. T., Faluvegi, G., and Bell, N.: Preindustrial-to-present-day radiative forcing by tropospheric ozone from improved simulations with the GISS chemistry-climate GCM, Atmos Chem Phys, 3, 1675–1702, https://doi.org/10.5194/acp-3-1675-2003, 2003.

Shindell, D. T., Faluvegi, G., Bell, N., and Schmidt, G. A.: An emissions-based view of climate forcing by methane and tropospheric ozone, Geophys Res Lett, 32, 1–4, https://doi.org/10.1029/2004GL021900, 2005.

Shindell, D. T., Faluvegi, G., Unger, N., Aguilar, E., Schmidt, G. A., Koch, D. M., Bauer, S. E., and Miller, R. L.: Simulations of preindustrial, present-day, and 2100 conditions in the NASA GISS composition and climate model G-PUCCINI, Atmos Chem Phys, 6, 4427–4459, https://doi.org/10.5194/acp-6-4427-2006, 2006.

Shindell, D. T., Pechony, O., Voulgarakis, A., Faluvegi, G., Nazarenko, L., Lamarque, J.-F., Bowman, K., Milly, G., Kovari, B., Ruedy, R., and Schmidt, G. A.: Interactive ozone and methane chemistry in GISS-E2 historical and future climate simulations, Atmos Chem Phys, 13, 2653–2689, https://doi.org/10.5194/acp-13-2653-2013, 2013.

Skeie, R. B., Berntsen, T. K., Myhre, G., Tanaka, K., Kvalevåg, M. M., and Hoyle, C. R.: Anthropogenic radiative forcing time series from pre-industrial times until 2010, Atmos Chem Phys, 11, 11827–11857, https://doi.org/10.5194/acp-11-11827-2011, 2011.

Skeie, R. B., Myhre, G., Hodnebrog, Ø., Cameron-Smith, P. J., Deushi, M., Hegglin, M. I., Horowitz, L. W., Kramer, R. J., Michou, M., Mills, M. J., Olivié, D. J. L., Connor, F. M. O., Paynter, D., Samset, B. H., Sellar, A., Shindell, D., Takemura, T., Tilmes, S., and Wu, T.: Historical total ozone radiative forcing derived from CMIP6 simulations, NPJ Clim Atmos Sci, 3, 32, https://doi.org/10.1038/s41612-020-00131-0, 2020.

Søvde, O. A., Hoyle, C. R., Myhre, G., and Isaksen, I. S. A.: The HNO_3 forming branch of the HO_2 + NO reaction: pre-industrial-to-present trends in atmospheric species and radiative forcings, Atmos Chem Phys, 11, 8929–8943, https://doi.org/10.5194/acp-11-8929-2011, 2011.

Stevenson, D. S., Johnson, C. E., Collins, W. J., Derwent, R. G., Shine, K. P., and Edwards, J. M.: Evolution of tropospheric ozone radiative forcing, Geophys Res Lett, 25, 3819–3822, https://doi.org/10.1029/1998GL900037, 1998.

Stevenson, D. S., Young, P. J., Naik, V., Lamarque, J.-F., Shindell, D. T., Voulgarakis, A., Skeie, R. B., Dalsoren, S. B., Myhre, G., Berntsen, T. K., Folberth, G. A., Rumbold, S. T., Collins, W. J., MacKenzie, I. A., Doherty, R. M., Zeng, G., van Noije, T. P. C., Strunk, A., Bergmann, D., Cameron-Smith, P., Plummer, D. A., Strode, S. A., Horowitz, L., Lee, Y. H., Szopa, S., Sudo, K., Nagashima, T., Josse, B., Cionni, I., Righi, M., Eyring, V., Conley, A., Bowman, K. W., Wild, O., and Archibald, A.: Tropospheric ozone changes, radiative forcing and attribution to emissions in the Atmospheric Chemistry and Climate Model Intercomparison Project (ACCMIP), Atmos Chem Phys, 13, 3063–3085, https://doi.org/10.5194/acp-13-3063-2013, 2013.

Tilmes, S., Hodzic, A., Emmons, L. K., Mills, M. J., Gettelman, A., Kinnison, D. E., Park, M., Lamarque, J. -F., Vitt, F., Shrivastava, M., Campuzano-Jost, P., Jimenez, J. L., and Liu, X.: Climate Forcing and Trends of Organic Aerosols in the Community Earth System Model (CESM2), J Adv Model Earth Syst, 11, 4323–4351, https://doi.org/10.1029/2019MS001827, 2019.

Tost, H., Jöckel, P., Kerkweg, A., Sander, R., and Lelieveld, J.: Technical note: A new comprehensive SCAVenging submodel for global atmospheric chemistry modelling, Atmos Chem Phys, 6, 565–574, https://doi.org/10.5194/acp-6-565-2006, 2006.

Walters, D., Baran, A. J., Boutle, I., Brooks, M., Earnshaw, P., Edwards, J., Furtado, K., Hill, P., Lock, A., Manners, J., Morcrette, C., Mulcahy, J., Sanchez, C., Smith, C., Stratton, R., Tennant, W., Tomassini, L., Van Weverberg, K., Vosper, S., Willett, M., Browse, J., Bushell, A., Carslaw, K., Dalvi, M., Essery, R., Gedney, N., Hardiman, S., Johnson, B., Johnson, C., Jones, A., Jones, C., Mann, G., Milton, S., Rumbold, H., Sellar, A., Ujiie, M., Whitall, M., Williams, K., and Zerroukat, M.: The Met Office Unified Model Global Atmosphere 7.0/7.1 and JULES Global Land 7.0 configurations, Geosci Model Dev, 12, 1909–1963, https://doi.org/10.5194/gmd-12-1909-2019, 2019.

Wang, H., Lu, X., Jacob, D. J., Cooper, O. R., Chang, K.-L., Li, K., Gao, M., Liu, Y., Sheng, B., Wu, K., Wu, T., Zhang, J., Sauvage, B., Nédélec, P., Blot, R., and Fan, S.: Global tropospheric ozone trends, attributions, and radiative impacts in 1995–2017: an integrated analysis using aircraft (IAGOS) observations, ozonesonde, and multi-decadal chemical model simulations, Atmos Chem Phys, 22, 13753–13782, https://doi.org/10.5194/acp-22-13753-2022, 2022.

Wang, X., Jacob, D. J., Downs, W., Zhai, S., Zhu, L., Shah, V., Holmes, C. D., Sherwen, T., Alexander, B., Evans, M. J., Eastham, S. D., Neuman, J. A., Veres, P. R., Koenig, T. K., Volkamer, R., Huey, L. G., Bannan, T. J., Percival, C. J., Lee, B. H., and Thornton, J. A.: Global tropospheric halogen (Cl, Br, I) chemistry and its impact on oxidants, Atmos Chem Phys, 21, 13973–13996, https://doi.org/10.5194/acp-21-13973-2021, 2021.

Wong, S., Wang, W. C., Isaksen, I. S. A., Berntsen, T. K., and Sundet, J. K.: A global climate-chemistry model study of present-day tropospheric chemistry and radiative forcing from changes in tropospheric O3 since the preindustrial period, Journal of Geophysical Research D: Atmospheres, 109, 11309, https://doi.org/10.1029/2003JD003998, 2004.

Zhao, M., Golaz, J. C., Held, I. M., Guo, H., Balaji, V., Benson, R., Chen, J. H., Chen, X., Donner, L. J., Dunne, J. P., Dunne, K., Durachta, J., Fan, S. M., Freidenreich, S. M., Garner, S. T., Ginoux, P., Harris, L. M., Horowitz, L. W., Krasting, J. P., Langenhorst, A. R., Liang, Z., Lin, P., Lin, S. J., Malyshev, S. L., Mason, E., Milly, P. C. D., Ming, Y., Naik, V., Paulot, F., Paynter, D., Phillipps, P., Radhakrishnan, A., Ramaswamy, V., Robinson, T., Schwarzkopf, D., Seman, C. J., Shevliakova, E., Shen, Z., Shin, H., Silvers, L. G., Wilson, J. R., Winton, M., Wittenberg, A. T., Wyman, B., and Xiang, B.: The GFDL Global Atmosphere and Land Model AM4.0/LM4.0: 2. Model Description, Sensitivity Studies, and Tuning Strategies, J Adv Model Earth Syst, 10, 735–769, https://doi.org/10.1002/2017MS001209, 2018.